1.1 Beam-beam simulation

Hyung Jin Kim
Mail to: hjkim@fnal.gov
Fermilab, MS220, P.O. BOX 500, Batavia, IL 60510

1.1.1 Introduction

In high energy storage-ring colliders, the beam-beam interactions are known to cause the emittance growth and the reduction of beam lifetime, and to limit the collider luminosity [1-6]. The long-range beam-beam effects can be mitigated by separating the beams to the extent possible. Increasing the crossing angle is a way of beam separation. It has several undesirable effects, the most important of which is a lower luminosity due to the smaller geometric overlap and the excitation of synchro-betatron resonance. In addition, in order to achieve a high luminosity, it needs to increase the beam intensity and often to focus the beam to smaller sizes at the interaction points. The effects of head-on interactions become even more significant. A tune spread is introduced by the head-on interactions due to a difference of tune shifts between small and large amplitude particles. The combination of beam-beam and machine nonlinearities excites betatron resonances which diffuse particles into the tail of beam distribution and even beyond the stability boundary.

It is therefore important to mitigate the beam-beam effects. Compensation of long-range beam-beam interactions by applying external electromagnetic forces has been proposed for the LHC [7]. At large beam-beam separation, the electromagnetic force which a beam exerts on individual particles of the other beam is proportional to $1/r$, which can be generated and canceled out by the magnetic field of a current-carrying wire. Direct-current wires were installed in SPS [7-9], DAΦNE [10], and later in RHIC [11] for tests. In the contrary, low energy electron beam, so called electron lens, has been used in the Tevatron at Fermilab to compensate the tune shift due to the beam-beam interaction [12-14]. The electron lens demonstrated the lifetime improvement of the Tevatron proton bunches. Its application to the mitigation of head-on beam-beam effects has been proposed recently in RHIC [15-16].

In this report we present an overview of computational model for beam-beam simulation, and its applications to both the long-range and head-on interactions in RHIC and LHC.

1.1.2 Computational model

In the collider simulation, the two beams moving in opposite direction are represented by macroparticles of which the charge to mass ratio is that of each beam. The number of macroparticles is much less than the bunch intensity of the beam because even with modern supercomputers it is too time consuming to track the particle inside the bunch, for example, 10^{11} particles for the number of revolutions of interest. The macroparticles are generated and loaded with an initial distribution for a specific simulation purpose, for example, six-dimensional Gaussian distribution for long-term

Operated by Fermi Research Alliance, LLC under Contract No. DE-AC02-07CH11359 with the United States Department of Energy

beam evolution. The transverse and longitudinal motion of particles is calculated by transfer maps which consist of linear and nonlinear maps.

The six-dimensional accelerator coordinates $\vec{x}=\left(x,x',y,y',z,\delta\right)^T$ are applied, where x and y are horizontal and vertical coordinates, x' and y' the trajectory slopes of each coordinates, $z=-c\Delta t$ the longitudinal distance from the synchronous particle, and $\delta=\Delta p/p_0$ the momentum deviation from the synchronous energy. Coupling between the transverse planes is included in the transfer map between elements. We adopt the weak-strong model to treat the beam-beam interactions where one beam is strong and is not affected by the other beam while the other beam is weak and experiences a beam-beam force due to the strong beam during the interactions. The density distribution of the strong beam is assumed to be Gaussian.

The bunch length effect needs to be considered in case of (1) the longitudinal bunch length σ_z is comparable to the transverse lengths σ_x and σ_y, (2) the orbit function β_x and β_y are not constant through beam-beam interactions, and (3) the transverse beta functions are small and comparable to σ_z. The finite longitudinal length is considered by dividing the beam into longitudinal slices. We make slices of both beams moving in opposite directions. Each slice is integrated over its longitudinal boundary, and has only transverse charge distribution at the center of its longitudinal boundary. We take into account the collision between a pair of slices: the ith slice of a beam and the jth slice of the other beam. The collision is taken place at collision point which is usually different from IP. For example, i^{th} the slice of a bunch has the successive collisions with slices of a bunch in the other beam. In addition, electric field energy varies along the bunch due to the inhomogenity of beam parameters in the longitudinal direction, and couples transverse and longitudinal motions. The coupling can be modeled by the synchro-betatron map which includes beam-beam interactions due to the longitudinal component of the electric field as well as the transverse components [17].

When there exists a finite crossing angle between colliding two beams at interaction point, the beam-beam force experienced by a test particle will have transverse and longitudinal components. The existence of longitudinal force makes it difficult to apply the result of no crossing angle. A transformation can be used to remedy the difficulty. It transforms a crossing angle collision in the laboratory frame to a head-on collision in the rotated and boosted frame which is called the head-on frame [18-19]. The transformation can be described by a transformation from the accelerator coordinates to Cartesian coordinates, the Lorentz transformation, and again a backward transformation to the accelerator coordinates.

It is well known that for a large separation distance at parasitic crossings, the strength of long-range interactions is inversely proportional to the distance, as shown Fig. 1. Its effect on a test beam can be compensated by current carrying wires which create just the $1/r$ field. The advantage of such an approach consists of the simplicity of the method and the possibility to deal with all multipole orders at once. For a finite length of a wire embedded in the middle of a drift length L, the change in slopes of a test beam at the wire is [20]

$$\begin{pmatrix}\Delta x'\\ \Delta y'\end{pmatrix}=\frac{\mu_0}{4\pi}\frac{I_w l_w}{B\rho}\frac{u-v}{x^2+y^2}\begin{pmatrix}x\\ y\end{pmatrix} \tag{1}$$

where I_w is the current of wire, u and v are $\sqrt{(L/2+l_w)^2+x^2+y^2}$ and $\sqrt{(L/2-l_w)^2+x^2+y^2}$ respectively. Taking into account the wire placement including pitch and yaw angles, the transfer map of a wire can be written as

$$M_w = S_{\Delta x,\Delta y} \circ T^{-1}_{\theta_x,\theta_y} \circ D_{L/2} \circ M_k \circ D_{L/2} \circ T_{\theta_x,\theta_y} \tag{2}$$

where T_{θ_x,θ_y} represents the tilt of the coordinate system by horizontal and vertical angles θ_x,θ_y to orient the coordinate system parallel to the wire, $D_{L/2}$ is the drift map with a length $L/2$, M_k is the wire kick integrated over a drift length, and $S_{\Delta x,\Delta y}$ represents a shift of the coordinate axes to make the coordinate systems after and before the wire agree. For cancelling the long-range beam-beam interactions of the round beam with the wire, one can get the desired wire current and length by equating the kicks from the wire and the strong beam at the large amplitude; the integrated strength of the wire compensator should be commensurate with the integrated current of the beam bunch, i.e., $(I_w l_w)=nqc$, where n is the beam intensity, q the beam charge, and c the speed of light.

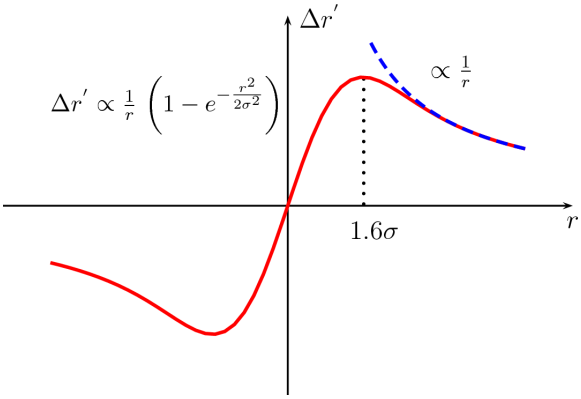

Figure 1: Beam-beam force of round Gaussian beam and a current-carrying wire.

A space charge force of low-energy electron beam is acting as a focusing or defocusing lens depending on the high energy bunch. A proton bunch colliding with a counterrotating proton bunch experiences a defocusing force which can be canceled out by a counterrotating electron beam having the same parameters as the counterrotating proton bunch. The transverse electron beam profile and its beam current are key parameters. The longitudinal electron beam profile is not really important because the betatron phase advance is negligible over the bunch length. Two electron beam distribution functions are commonly considered as shown in Fig. 2.: (i) Gaussian distribution and (ii) Smooth-edge-flat-top (SEFT) distribution. The transverse kick on the high energy beam from the electron beam is given by

$$\Delta \vec{r}' = \frac{2nr_0}{\gamma}\frac{\vec{r}_\perp}{r_\perp^2}\zeta(r_\perp:\sigma) \tag{3}$$

where n is the number of electrons of the electron beam adjusted by the electron speed, r_0 is the classic proton radius, and γ is the Lorentz factor. The function ζ is given by

- for Gaussian distribution

$$\zeta = 1 - \exp\left(-\frac{r_\perp^2}{2\sigma^2}\right) \tag{4}$$

- for SEFT distribution

$$\zeta = \frac{\sqrt{2}\,\rho_0}{8}\left[\frac{1}{2}\log\left(\frac{\theta_+^2+1}{\theta_-^2+1}\right) + \tan^{-1}\theta_+ + \tan^{-1}\theta_-\right] \tag{5}$$

where ρ_0 is a constant, and $\theta_\pm = \sqrt{2}\,(r/\sigma)^2 \pm 1$.

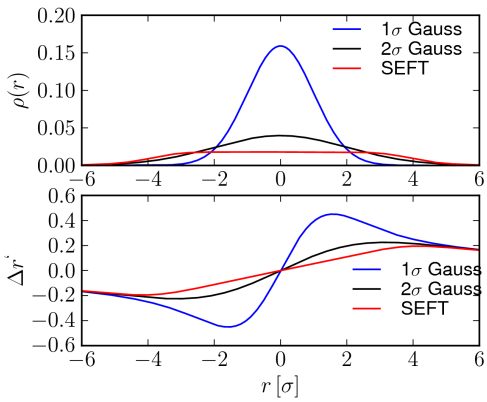

Figure 2: (top) Transverse electron beam distributions: (black) $2\sigma_p$ Gaussian distribution, (blue) $2\sigma_p$ Gaussian distribution, and (red) constant distribution with smooth edge; $\rho(r) \sim 1/(1+(r/4\sigma_p)^8)$. (bottom) Kicks from the electron beam distribution. Note that the number of particles of three distribution is the same.

Following the above physical model, a beam-beam simulation code BBSIMC has been developed at FNAL over the past few years to study the effects of the machine nonlinearities and the beam-beam interactions [21]. If required, time dependent effects such as tune modulation and fluctuation, beam offset modulation and fluctuation, dipole strength fluctuations to mimic rest-gas scattering etc can be included in the model. The code is under continuous development with the emphasis being on including the important details of an accelerator and the ability to reproduce observations in diagnostic devices. At present, the code can be used to calculate tune footprints, dynamic apertures, beam transfer functions, frequency diffusion maps, action diffusion coefficients, emittance growth and beam lifetime. Calculation of the last two quantities over the long time scales of interest is time consuming even with modern computer technology. In order to run efficiently on a multiprocessor system, the resulting model was implemented by using parallel libraries which are interprocessor Message Passing Interface standard [22] and Portable, Extensible Toolkit for Scientific Calculation [23].

1.1.3 Applications

Relativistic Heady Ion Collider

At store energy the Relativistic Heavy Ion Collider (RHIC) has nominally two head-on beam-beam collisions at IP6 and IP8. There are no long-range interactions. In order to investigate the long-range beam-beam interactions and test the compensation scheme, two current carrying wires, one for each beam, were installed between the magnets Q3 and Q4 of IP6 in the RHIC tunnel [11]. The impact of a wire can be observed by measuring the orbit change, tune shift, the beam transfer function and the loss rates. The tune shift is one of the fundamental observables and it can be directly verified with analytical calculation. However, numerical simulations allow us to calculate other quantities not easily observable but which give valuable insight into the beam dynamics and can complement the experiments. These numerically calculable quantities include the tune footprint, the frequency diffusion map, the dynamic aperture, and the diffusion coefficients to characterize the diffusion in action. These are discussed in detail in ref. [21]. In this letter we will present the effect of the wire on the beam loss rates as the beam-wire separation is changed. In the simulation, the loss rates are estimated from the asymptotic limit by extrapolating the simulated loss rate because in the beginning of the simulation, the loss rate decreases exponentially rapidly and then approaches a constant rate at later times. The onset of beam losses, seen in Fig. 3, is observed at 8 σ and 9 σ for gold and deuteron beams respectively. In both cases, the threshold separation for the onset of sharp losses observed in the measurements and simulations agree to better than 1 σ. It is also significant that the simulated loss rates at 7 σ and 8 σ separations for the gold beam and 8 σ and 9 σ for the deuteron beam are very close to the measured loss rates.

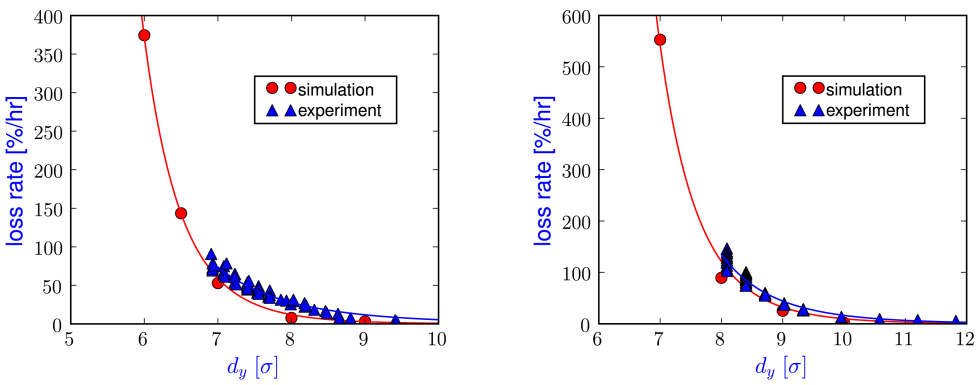

Figure 3: Comparison of the simulated beam loss rates with the measured as a function of separations. (left) gold beam at collision energy, (right) deuteron beam at collision energy. Wire strength is 125 Am.

The electron lens has been proposed in particular for a reduction of the large tune spread of proton beam and emittance growth in RHIC [15,16]. The tune spread can be fully compressed by the electron lens with an electron beam profile which matches to a proton beam. Simulation studies, however, showed that the electron lens leads to an increase of beam loss when the electron beam profile matches a proton beam at the lens location and its intensity is chosen to fully compress the tune spread [24]. The full compensation of betatron tune is not a necessary and sufficient condition for improving

the beam lifetime because the beam stability can get worse from footprint folding. In order to investigate the effects of different electron lens profiles and intensities on the beam dynamics, we calculated dynamic apertures, frequency diffusion maps, and particle loss [25,26]. We observed a small increase in the dynamic aperture of off-momentum particles at small compensation strength. There is however a significant reduction in beam loss. A wider electron beam profile than the proton beam at the electron lens location is found to increase beam life time. In addition, the tune scan shows that the electron lens reduces the particle loss over the wide range of betatron tune for wide electron beam profile while no increase of beam lifetime is indicated for 1 σ Gaussian profile, as shown in Fig. 4. This looser tolerance on the allowed variations in electron intensity is likely to be beneficial during experiments.

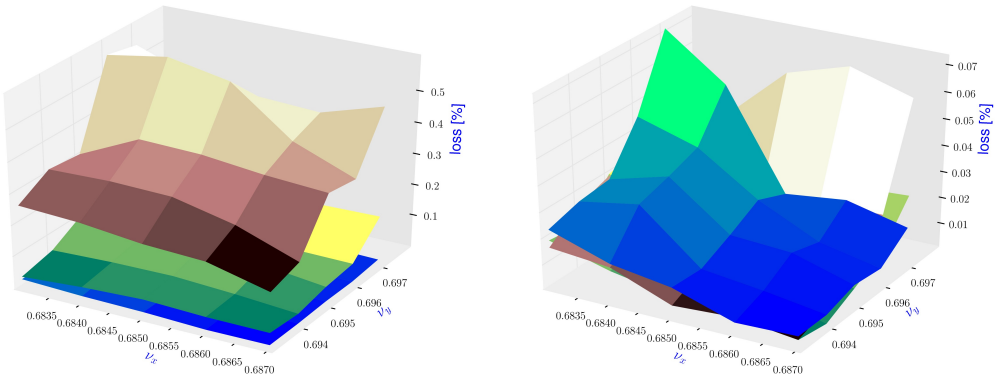

Figure 4: Plot of beam loss relative to the loss of no wire case: (left) 1σ Gaussian and (right) SEFT electron lens.

<u>Large Hadron Collider</u>

The Large Hadron Collider (LHC) has at most four interaction points. Due to the design goal of highest luminosity, the LHC operates with a large number of bunches at high intensities. The beams in the LHC experience a large number of up to 120 long-range interactions on either side of collision points. The long-range interaction is expected to limit the LHC performance. In order to mitigate the nonlinear effect of the long-range collisions, one can employ a current-carrying wire at the location of the long-range encounters. The wire's locations are proposed where the beta functions in both transverse planes are equal [6]. The average phase advance between the location of the wire and the location of the long-range interaction points is about 3º. The integrated current for optimal tune compression is 82.8 Am. At the nominal LHC the beam-beam separation distance normalized by the transverse rms bunch size varies from 6.3 σ to 12.6 σ and is asymmetric with respect to the interaction points. The resulting beam-beam force is not identical to that generated by a single or multiple wire(s). The wire-beam separation distance is therefore one of major parameters which determine the performance of a wire compensator. Figure 5 shows the results of proton beam loss for different wire-beam separations. The particle loss saturates at large separation while there is a sharp increase of particle loss at small separation. The minimum particle loss

is observed between 8 σ and 9 σ wire-beam separations which are close to the averaged beam-beam separation on each side of the interaction points.

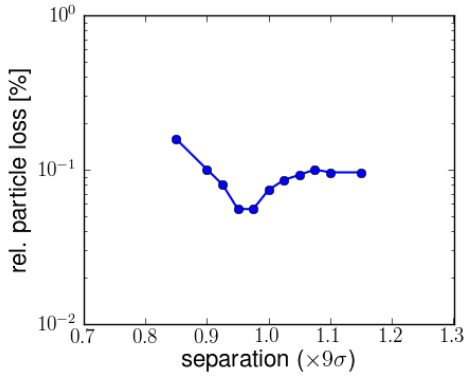

Figure 5: Plot of particle loss according to wire-beam separation distance with wire strength 82.8 Am.

1.1.4 Acknowledgements

Some of the parallel computations were performed at the NERSC facility at LBL and the CARC at UNM. This work was supported by the US-LARP collaboration which is funded by the US Department of Energy.

1.1.5 References

1. T. Sen, B. Erdelyi, M. Xiao, and V. Boocha, Phys. Rev. ST Accel. Beams **7**, 41001 (2004).
2. V. Shiltsev, Y. Alexahin, V. Lebedev, P. Lebrun, R. S. Moore, T. Sen, A. Tollestrup, A. Valishev, and X. L. Zhang, Phys. Rev. ST Accel. Beams **8**, 101001 (2005).
3. A. Valishev, Proceedings of EPAC08, p. 2937 (2008).
4. V. Ptitsyn et al., Proceedings EPAC06, p. 592 (2006).
5. K. Ohmi, Proceedings of EPAC08, p. 2593 (2008).
6. J.-P. Koutchouk, Proceedings of PAC07, p. 3387 (2007).
7. J. P. Koutchouk, J. Wenninger, and F. Zimmermann, Proceedings of EPAC04, p. 1936 (2004).
8. U. Dorda, J. Koutchouk, R. Tomas, J. Wenninger, F. Zimmermann, R. Calaga, and W. Fischer, Proceedings of EPAC08, p. 3176 (2008).
9. F. Zimmermann, J.-P. Koutchouk, F. Roncarolo, J. Wenninger, T. Sen, V. Shiltsev, and Y. Papaphilippou, Proceedings of PAC05, p. 686 (2005).
10. C. Milardi, D. Alesini, M. A. Preger, P. Raimondi, M. Zobov, and D. Shatilov, Proceedings of CARE-HHH- APD IR07 Workshop, p. 92 (2007).
11. W. Fischer et al., Proceedings of PAC07, p. 1859 (2007).
12. V. Shiltsev, Y. Alexahin, K. Bishofberger, V. Kamerdzhiev, G. Kuznetsov, and X.-L. Zhang, Physical Review Letters, **99**, 244801 (2007).
13. V.Kamerdzhiev, Yu.Alexahin, V.Shiltsev, A.Valishev, and XL.Zhang, Proceedings of PAC07, p. 1703 (2007).

14. V Shiltsev et al, New Journal of Physics, **10**, 043042 (2008).
15. Y. Luo and W. Fischer, BNL-CAD/AP/286 (2007).
16. Y. Luo, W. Fischer, and N. Abreu, BNL C-A/AP/310 (2008).
17. K. Hirata, H. Moshammer, and F. Ruggiero, Part. Accel. 40, 205 (1993).
18. K. Hirata, SLAC-PUB-637 (1994).
19. L. Leunissen, F. Schmidt, and G. Ripken, Phys. Rev. ST Accel. Beams **3**, 124002 (2000).
20. B. Erdelyi and T. Sen, Fermilab-TM-2268-AD, (2004).
21. H.J. Kim, T. Sen, N. P. Abreu, and W. Fischer, PRST-AB **12**, 031001 (2009).
22. MPI-2: Extensions to the Message-Passing Interface, Message Passing Interface Forum, University of Tennessee (2003).
23. S. Balay, W. D. Gropp, L. C. McInnes, and B. F. Smith, ANL-95/11, Revision 2.3.3 (2008).
24. A. Valishev et al., LARP Mini-Workshop on Electron Lens Simulations at BNL (2008).
25. H.J. Kim and T. Sen, Proceedings of PAC09, WE6PFP032 (2009).
26. H.J. Kim and T. Sen, Proceedings of IPAC10, p. 2075 (2010).